

Quantitative study of magnetic field distribution by electron holography and micromagnetic simulations

M. Beleggia,^{a)} M. A. Schofield, and Y. Zhu

Materials Science Department, Brookhaven National Laboratory, Upton, New York 11973

M. Malac, Z. Liu, and M. Freeman

Department of Physics, University of Alberta, Edmonton, T6G 2J1, Canada

(Received 24 February 2003; accepted 20 June 2003)

The magnetic configuration of a submicrometer Ni₈₈Fe₁₂ permalloy island has been quantitatively mapped by off-axis electron holography. The two main contributions to the electron-optical phase shift, namely the phase shifts induced by the electrostatic and magnetic potentials, including fringing fields, were separated by inverting the specimen of 180° with respect to the electron beam and directly measuring the mean inner potential. A quantitative map of the projected magnetic induction in the sample was thereby retrieved and compared to results of micromagnetic and electromagnetics calculations, providing the minimum-energy configuration and the phase shift, respectively. © 2003 American Institute of Physics. [DOI: 10.1063/1.1603355]

Domain configuration of magnetic structures at nanometric scale and interparticle coupling within regular arrays of such structures is subject of intensive research.¹ The continuously decreasing size of magnetic elements in magnetic storage media provides perhaps the strongest motivation for this activity.² However, there are still many fundamental scientific issues to be addressed. In many instances information on both direction of magnetization and field intensity is necessary to understand the fundamental properties and behavior of such systems. Among the many techniques available for mapping magnetic fields (see Ref. 3) electron holography offers the opportunity to map fields with spatial resolution down to few nanometers⁴ and phase sensitivity of the order of $\pi/100$.⁵ The most important advantage of electron holography is the quantitative phase shift retrieval, which includes information on the magnetization throughout the specimen as well as on the fringing field in the regions above and below the sample. The electron beam passing through a sample undergoes an electron-optical phase shift due to the presence of electrostatic and magnetic potentials, and can be evaluated as the integral of the potentials along the electron trajectory. To unravel the respective contributions it is necessary to provide a way to separate the electrostatic and magnetic components to the phase shift. This is particularly important when small scales are involved, as the ratio between the components does not allow us to neglect either of them.⁶

To take full advantage of measurements performed in a transmission electron microscope (TEM), it is important to relate experimental results to the output of micromagnetic simulations. However, achieving quantitative agreement between experimental data and results of micromagnetic simulations remains problematic.⁷ In fact, both the sample and the modeled data need to refer to a sample with exactly the same geometry, history, and experimental conditions. The second requirement may be relaxed if a match of experiment and

simulation is attempted on a sample in a well defined state. The easiest approach is to try to match both the sample and the simulations for a magnetic element in the ground state (lowest energy) configuration. Further difficulties can arise if multiple structures are situated in close proximity as they can both influence the configuration of the ground state and distort the reference wave in the electron holography experiments. This makes both the micromagnetic simulations and reconstruction of electron holography data more difficult. We have used Landau–Lifshitz–Gilbert (LLG) equations⁸ to model the magnetic configuration of the sample. Even though this is a macroscopic, phenomenological approach (often used to simulate dynamic behavior of magnetic switching), it is well-suited for the calculation of equilibrium states of submicron structures. Results of such micromagnetic simulations were used to compute the phase shift induced on the electron wave front.

Thin film samples of permalloy squares and rectangles on 50-nm-thick silicon nitride membrane were prepared by electron beam patterning of poly(methyl methacrylate) photoresist followed by lift-off of a sputter deposited film. The permalloy film was deposited in a field-free environment. To prevent charging in the electron beam the sample was coated with a 2-nm-thick, amorphous carbon layer. The composition of the permalloy film was measured to be Ni 88% Fe 12% by electron energy loss spectroscopy using a JEOL 3000F TEM. We estimate the accuracy of the composition to be 10% of the measured values based on inaccuracies of background subtraction and inelastic cross-section calculation.⁹

In order to retrieve the values of local magnetization and mean inner potential, the local thickness of the sample has to be measured. To address this concern we have measured the thickness distribution by energy filtered imaging. The zero-loss filtered image was collected with energy selecting slit width of 3 eV and an unfiltered image was collected from the same area. The two images, aligned by standard cross-correlation methods, can then be converted to a thickness map according to⁹

^{a)}Author to whom correspondence should be addressed; electronic mail: beleggia@bnl.gov

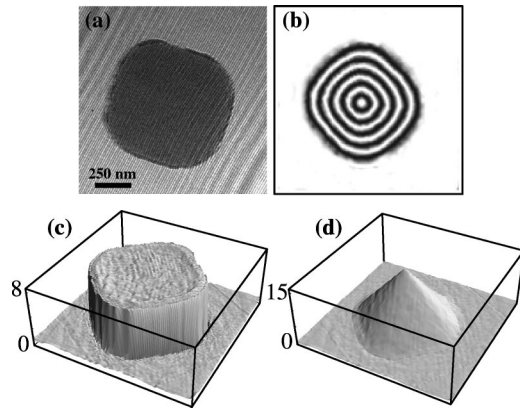


FIG. 1. (a) Electron hologram of the magnetic element; (b) contour map ($2\times$ amplified) of the total phase shift; (c) electrostatic and (d) magnetic contributions to the phase shift (in radians) retrieved from the experiment.

$$t(x,y) = \lambda \log \frac{I(x,y)}{I_0(x,y)}, \quad (1)$$

where λ is the inelastic mean free path (MFP) of the material and $I(x,y)$ and $I_0(x,y)$ are the unfiltered and filtered image intensities, respectively.

For permalloy $\text{Ni}_{88}\text{Fe}_{12}$, 300 kV incident beam energy and 10 mrad collection semiangle, λ was estimated to be 119 nm using the empirical formula by Malis.¹⁰ Since the values of inelastic mean free paths are additive⁹ the permalloy thickness has been retrieved by subtracting the substrate (SiN+C) thickness from the total thickness, thus giving a permalloy thickness of 0.38 MFP, or (45 ± 5) nm with the estimated value of λ . This is in good agreement with the thickness expected from *in situ* measurements by crystal film thickness monitor.

Electron holograms were recorded to measure the electron phase shifts induced by the sample. A set of two holograms was acquired with sample flipped between the acquisitions. The difference and sum of the two phase images, shown in Figs. 1(c) and 1(d), allowed us to quantitatively separate the magnetic and electrostatic contributions to the phase shifts.¹¹ The sample was studied at room temperature with the main objective lens off. The weak remnant field of the lens (0.02 T perpendicular to the sample plane) did not change the magnetic configuration of the element. From the electrostatic component of the phase shift, and using the measured thickness, we estimate the mean inner potential of permalloy to be (26 ± 3) V.

Micromagnetic simulations based on LLG equations were performed on the element. The choice of the initial state and of the damping parameter of the LLG simulations affect the calculated equilibrium state. As an initial configuration, we used a random magnetization, as shown in Fig. 2.

We also note the importance of matching the shape of the modeled element to the real one. To achieve the best possible match we used the in-focus image of the element as a template to define the shape in the micromagnetic simulation. The damping constant α was taken to be 0.008 while the exchange constant A was taken to be 10^{-6} erg/cm. The main influence of the damping constant appears to be the rate of convergence of the computation. A large value of α results in the possibility that the simulation converges to a local

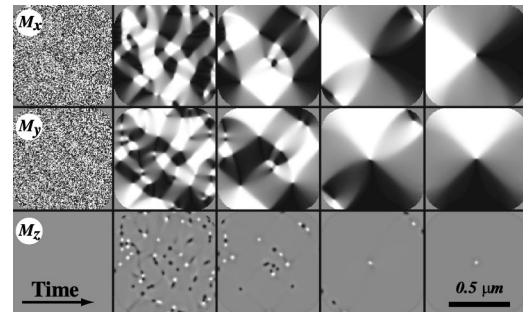


FIG. 2. Micromagnetic simulations on the element: an initial random magnetization (left) evolves to a vortex state (right). The element size is 830×855 nm.

minimum rather than the global minimum of magnetic energy (ground state configuration). Since the crystalline size in our sample is of the order of 10 nm, and the film was deposited at zero applied field, we have assumed the magnetocrystalline anisotropy to be zero.

In order to describe the phase shift induced on the electron beam by the electromagnetic field associated to the element, we make use of the standard Aharonov–Bohm expression

$$\varphi = \varphi_e + \varphi_m = C_E \int V dz - \frac{\pi}{\phi_0} \int A_z dz, \quad (2)$$

where $C_E = 6.25 \times 10^{-3} \text{ V}^{-1} \text{ nm}^{-1}$ for 300 kV electrons and ϕ_0 is the flux quantum $h/2e = 2.07 \times 10^3 \text{ T nm}^2$.

The electrostatic contribution can be written as $\varphi_e = C_E V_0 t(x,y)$ where V_0 is the mean inner potential and $t(x,y)$ is the thickness profile of the element.

The magnetic component φ_m can be calculated analytically from the knowledge of the vector potential, or numerically from the knowledge of the magnetization configuration. As was emphasized in Ref. 6 the analytical calculation can be performed only for simple geometries. In the general case, especially when domain walls or vortices are present in the magnetic structure, if the magnetization is available from micromagnetic simulations, we can calculate the phase shift by extending the Fourier space approach recently introduced.^{6,12} From the knowledge of the two in-plane magnetization components (m_x, m_y) we can express the z component of the vector potential in a (k_x, k_y, k_z) Fourier space as

$$\tilde{A}_z = - \frac{2i\mu_0 M_0}{k_z} \frac{\tilde{m}_x k_y - \tilde{m}_y k_x}{k_x^2 + k_y^2 + k_z^2} \sin(k_z t/2), \quad (3)$$

where $(\tilde{m}_x, \tilde{m}_y)$ are the numerical fast Fourier transform (FFT) of (m_x, m_y) . Integrating Eq. (3) along the optical axis z we can calculate the phase shift. The Fourier representation of the phase shift turns out to be

$$\tilde{\varphi}_m = \frac{i\pi\mu_0 M_0 t}{\phi_0} \frac{\tilde{m}_x k_y - \tilde{m}_y k_x}{k_x^2 + k_y^2}. \quad (4)$$

The resulting phase shift, obtained by an inverse FFT of Eq. (4) and corresponding to the last four states in Fig. 2 are shown in Fig. 3. It can be noticed that the agreement between the expected final state shown in Fig. 1(d) and the measured magnetic configuration of the element reported in Fig. 1(d) is excellent. The phase variations visible outside the element, Downloaded 21 Aug 2003 to 130.199.3.3. Redistribution subject to AIP license or copyright, see http://ojps.aip.org/aplo/aplcr.jsp

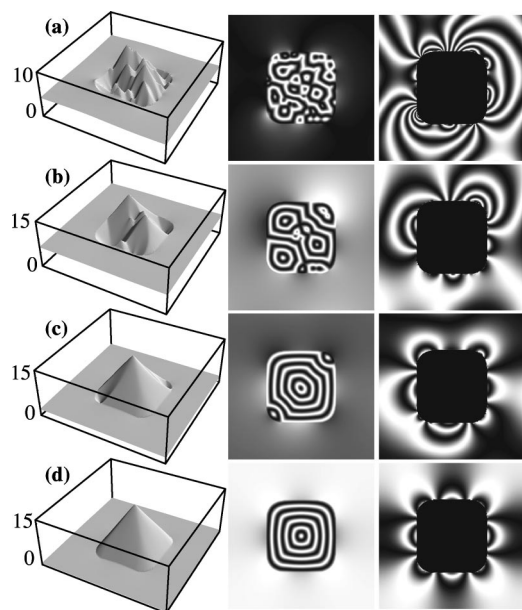


FIG. 3. Phase shift from micromagnetic simulations (last four states of Fig. 2) displayed as three-dimensional plot (first column), $2\times$ (second column), and $32\times$ (third column) amplified contour maps.

emphasized in the $32\times$ amplified contour map displayed in the third column, can be ascribed to fringing fields. It can be noticed that part of the magnetic field leaks to the vacuum outside. The opportunity to take into account correctly the fringing fields surrounding magnetic elements is the key to a truly quantitative magnetization mapping. It also represents a difference between this work and similar papers in the literature (see, e.g., Refs. 13–15). If the fringing fields are neglected, the measurements of the local induction, in terms of field intensity and direction, are either dramatically limited to perfect closure-domain states, almost never present when small dimensions are involved, or unavoidably spoiled by the projection of the electron beam onto the specimen.

It has been shown how a combination of electron holography, electron energy loss spectroscopy, micromagnetic

simulation and theoretical modeling allows us to obtain all the necessary information regarding the magnetic configuration of elements on the nanometric scale. The limit of electron holography, which in terms of retrieving the magnetic signal from nanoparticles can be in principle of the order of 10 nm in particle size, has not yet been reached. Experiments are now in progress to push observations to the scale where transmission electron microscopy is the only technique available for the characterization of magnetic properties of individual nanoparticles.

This work was supported by U.S. Department of Energy, Basic Energy Science, under Contract No. DE-AC02-98CH10886, by iCORE (Province Alberta), and by the Natural Science and Engineering Research Council of Canada. The authors gratefully acknowledge the invaluable technical support given by M. Aktary.

¹R. P. Cowburn and M. E. Welland, *Science* (Washington, DC) **287**, 1466 (2000).

²K. O'Grady and H. Laider, *J. Magn. Magn. Mater.* **200**, 616 (1999).

³E. Dahlberg and R. Proksch, *J. Magn. Magn. Mater.* **200**, 720 (1999).

⁴*Introduction to Electron Holography*, edited by E. Völkl, L. Allard and D. C. Joy (Kluwer Academic, Dordrecht, 1999).

⁵A. Tonomura, *Electron Holography* (Springer, Berlin, 1993).

⁶M. Beleggia and Y. Zhu, *Philos. Mag. B* **83**, 1043 (2003)

⁷R. E. Dunin-Borkowsky, M. R. McCartney, D. J. Smith, and S. Parkins, *Ultramicroscopy* **74**, 61 (1998).

⁸Y. Nakatani, Y. Uesaka, and N. Hayashi, *Jpn. J. Appl. Phys., Part 1* **28**, 2485 (1989).

⁹R. Egerton, *Electron Energy-Loss Spectroscopy in the Electron Microscope*, 2nd ed. (Plenum, New York, 1996).

¹⁰T. Malis, S. C. Cheng, and R. F. Egerton, *J. Electron Microsc. Tech.* **8**, 193 (1988).

¹¹A. Tonomura, T. Matsuda, J. Endo, and K. Mikama, *Phys. Rev. B* **34**, 3397 (1986).

¹²M. Beleggia, P. F. Fazzini, and G. Pozzi, *Ultramicroscopy* **96**, 93 (2003).

¹³S. McVitie, G. S. White, J. Scott, P. Warin, and J. N. Chapman, *J. Appl. Phys.* **90**, 5220 (2001).

¹⁴M. R. McCartney and Y. Zhu, *J. Appl. Phys.* **83**, 6414 (1998).

¹⁵R. E. Dunin-Borkowski, M. R. McCartney, B. Kardynal, D. J. Smith, and M. R. Scheinfein, *Appl. Phys. Lett.* **75**, 2641 (1999).